In-plane uniaxial strain in black phosphorus enables the identification of crystalline orientation

Shuqing Zhang, Nannan Mao, Juanxia Wu, Lianming Tong, Jin Zhang,* and Zhirong Liu**

S. Zhang, N. Mao, Dr. J. Wu, Dr. L. Tong, Prof. J. Zhang, Prof. Z. Liu
Center for Nanochemistry, College of Chemistry and Molecular Engineering, Peking University, Beijing 100871, P. R. China
S. Zhang, Prof. J. Zhang, Prof. Z. Liu
Academy for Advanced Interdisciplinary Studies, Peking University, Beijing, 100871, P. R. China
E-mail: tonglm@pku.edu.cn; jinzhang@pku.edu.cn; liuzhirong@pku.edu.cn

Keywords: black phosphorus, Raman shifts, strain effects, crystalline orientation

Abstract

The identification of the crystalline axis of anisotropic black phosphorus (BP) is key for the study of its physical properties and for its optical and electronic applications. Herein, we show that by applying an in-plane uniaxial strain and measuring the changes of Raman shifts, the crystalline axis of BP can be reliably determined. The strain effects on Raman shifts are angle-dependent, which can be expressed as a combination of Raman responses under zigzag and armchair strains. Different from previous polarized optical spectroscopic means, the proposed method does not rely on the laser polarization, the excitation wavelength, the sample thickness and the material of the stretchable substrate. Besides, the effective strain applied on BP from the stretched substrate is estimated, showing that only 20% to 40% of the strain can be effectively transferred to BP flakes from polyethylene terephthalate substrates. Our method provides not only an effective and universal approach to identify the crystalline orientation of layered BP, but also a model to extract additional information in strain-related studies, and can be extended to other 2D anisotropic materials.

1. Introduction

Black phosphorus (BP) is the most stable allotrope form of crystalline phosphorus, and it is black and flaky as graphite.[1,2] Few-layer BP has many attractive features. For example, its bandgap is thickness-dependent and can be tuned from 0.3 eV to around 2 eV,[3,4] and the charge carrier mobility may exceed 1000 $cm^2 V^{-1} s^{-1}$ at room temperature and even tens of thousands at lower temperature.[5,6] Therefore, it has attracted tremendous interest since 2014.[7-9] Different from isotropic two-dimensional (2D) materials such as graphene and some transition metal dichalcogenides, BP is anisotropic with orthorhombic structure. Its mechanical behavior,[10] electrical mobility,[11,12] optical absorption[11,13] and thermoelectric[14] properties all depends on the crystalline orientation in space. To take advantage of the desirable anisotropic properties of BP and other anisotropic 2D materials, a non-destructive, effective and universal characterization tool to identify the crystalline orientation has become the urgent need.

Raman spectroscopy is a fast and non-destructive characterization method. The peak positions, intensities and shapes of bands in Raman spectroscopy contain enormous information about the atomic structure, existing forms, defects, electronic and phonon properties of the samples, making it a necessary and standardized technique in the study of 2D materials.[15-17] Based on the conventional selection rules of orthorhombic system, the intensity distributions from Raman tensors are angle-resolved, so the polarized Raman spectroscopy was regarded as a possible tool for identifying the crystalline orientation of BP layers in the earlier studies.[18-20] However, it was later revealed that the excitation wavelength and sample thickness both played important roles in the angle-dependent Raman intensity of BP crystals,[13,21,22] which complicates the orientation identification by polarized Raman method where complex intrinsic electron-photon and electron-phonon interactions have to be taken into account.[13] Here, we shift our focus from peak intensity to another important factor, the Raman shift, which is mainly determined by overall crystal structure and the bond length and angle, but not by the optical effects or interference effects from excitation laser energy

and the thickness of BP flakes.[7,23-25] We will show that the changes of Raman shift under in-plane uniaxial strain are angle-dependent, and it can be used to reliably determine the crystalline orientation of BP samples.

The main idea is briefly sketched in **Figure 1**. The structure of monolayer BP is highly anisotropic (Figure 1a and Figure S1), forming a strongly puckered honeycomb lattice with troughs running in a zigzag (ZZ) direction. The three usual characteristic Raman bands of BP films locate around 360 cm^{-1}, 440 cm^{-1} and 470 cm^{-1} (Figure 1c), which are attributed to A_g^1, B_{2g} and A_g^2 modes, respectively. Under an in-plane uniaxial strain (with the orientation angle denoted as θ in Figure 1b), the Raman shifts have obvious changes compared with the unstrained case (Figure 1c). The frequency changes versus strain are angular dependence (solid curves in Figure 1d). By comprehensively considering the shift patterns of the three bands under a sole strain (instead of the shift amplitude of one band since the actual strain in 2D system is often overestimated[24,26,27]), the angle θ of strain and the crystalline orientation can be readily determined as explained in details in the rest of this paper.

2. Results and Discussion

2.1. Model of orientation-dependent Raman frequency shifts versus strain

Strain is a second-order tensor, and it can be written in a skew symmetric matrix in 2D system:

$$\boldsymbol{\varepsilon} = \begin{bmatrix} \varepsilon_{xx} & \varepsilon_{xz} \\ \varepsilon_{xz} & \varepsilon_{zz} \end{bmatrix}, \tag{1}$$

where ε_{xx} and ε_{zz} are the uniaxial strain along the *x* and *z* axes, respectively, while ε_{xz} is the shear strain component. For a uniaxial strain $\boldsymbol{\varepsilon}$ along any specified direction with angle θ, it can be expressed by a rotation transformation as:

$$\boldsymbol{\varepsilon}(\theta) = \begin{bmatrix} \varepsilon_{xx} & \varepsilon_{xz} \\ \varepsilon_{xz} & \varepsilon_{zz} \end{bmatrix} = \mathbf{R}^T \begin{bmatrix} \varepsilon & 0 \\ 0 & 0 \end{bmatrix} \mathbf{R} = \begin{bmatrix} \varepsilon\cos^2\theta & -\varepsilon\sin\theta\cos\theta \\ -\varepsilon\sin\theta\cos\theta & \varepsilon\sin^2\theta \end{bmatrix}, \tag{2}$$

where **R** is the 2D rotation matrix:

$$\mathbf{R} = \begin{bmatrix} \cos\theta & \sin\theta \\ -\sin\theta & \cos\theta \end{bmatrix}. \quad (3)$$

When the applied strain is small, the phonon frequency changes linearly with the strain,[28] and for non-degenerate modes as those in BP, it simply reads:

$$\omega(\varepsilon,\theta) = \omega_0 + k_x\varepsilon_{xx} + k_z\varepsilon_{zz} + 2k_\gamma\varepsilon_{xz} = \omega_0 + (k_x\cos^2\theta + k_z\sin^2\theta - 2k_\gamma\sin\theta\cos\theta)\varepsilon, \quad (4)$$

where k_x and k_z are the change rates of the frequencies versus strain along ZZ and AC directions, respectively, and k_γ is the rate under shear strain. Due to the mirror reflection symmetry (perpendicular to *xz*-plane) of orthorhombic structure, the frequency remains invariant under opposite shear strain [$\omega(\varepsilon_{xz},\theta) \rightarrow \omega(-\varepsilon_{xz},\theta)$], so the contribution of shear strain to the frequency change is zero, i.e.,

$$k_\gamma = 0. \quad (5)$$

Therefore, the frequency under a uniaxial strain with a directional angle θ becomes

$$\omega(\varepsilon,\theta) = \omega_0 + (k_x\cos^2\theta + k_z\sin^2\theta)\varepsilon. \quad (6)$$

So the change rate of frequency versus strain is angle-dependent:

$$k = \frac{\partial\omega}{\partial\varepsilon} = k_x\cos^2\theta + k_z\sin^2\theta. \quad (7)$$

For monolayer BP, the Raman shifts of A_g^1, B_{2g} and A_g^2 modes under uniaxial strains along ZZ and AC directions are calculated with density-functional theory (DFT) (See Calculation Methods and Supporting Information for details) and summarized in **Figure 2**a–c. The frequencies of other optical phonons at the center of Brillouin zone of monolayer BP are listed in Figure S4. It can be seen that the change rates are different for the three modes. For A_g^1 mode, the change under AC strain is larger than that under ZZ strain, while for B_{2g} and A_g^2 modes, the Raman shifts changed very little with AC strain, but show much larger shifts by ZZ strain. These features can be explained by the changes of geometric

parameters under the two typical directions.[24,25] As shown in the inset of Figure 1c, the atomic displacements of the modes are mainly contributed by relative vibration of the atoms within the layer, which are not sensitive to interlayer coupling. As a result, both calculations and experiments have shown that the Raman shifts of few-layer BP almost unchanged for different flakes with distinct thickness.[7,23,24]

According to Equation 7, the change rates at any angle θ can be derived from the frequency responses along ZZ direction (k_x) and AC direction (k_z). In Figure 2d-f, we draw the results of Equation 7 as solid lines using k_x and k_z determined in Figure 2a-c, and compare them with the values obtained with direct DFT calculations at each θ (scattering points). The agreement is excellent, supporting the validity of Equation 7. The results of other optical phonons, such as B_{1g}, B_{3g} and A_u modes, are shown in Figure S4 and Figure S5 in Supporting Information.

2.2. Determining the crystalline orientation of BP by the change rates of Raman shifts

From Equation 7, the change rates of three Raman modes are θ-dependent as

$$\begin{cases} k_1(A_g^1) = k_{1x}\cos^2\theta + k_{1z}\sin^2\theta \\ k_2(B_{2g}) = k_{2x}\cos^2\theta + k_{2z}\sin^2\theta \\ k_3(A_g^2) = k_{3x}\cos^2\theta + k_{3z}\sin^2\theta \end{cases}. \quad (8)$$

where subscripts 1, 2 and 3 denote A_g^1, B_{2g} and A_g^2 modes, respectively. To facilitate the deduction, we rewrite there change rates into a three-component vector, i.e.,

$$\vec{k} = \begin{pmatrix} k_1 \\ k_2 \\ k_3 \end{pmatrix}, \ \vec{A} = \begin{pmatrix} k_{1x} \\ k_{2x} \\ k_{3x} \end{pmatrix}, \ \vec{B} = \begin{pmatrix} k_{1z} \\ k_{2z} \\ k_{3z} \end{pmatrix}. \quad (9)$$

Components of $\vec{A}$ and $\vec{B}$ were listed in Figure 2a-c. Any three-component vector $\vec{k}$ can be written as a combination of ($\vec{A}$, $\vec{B}$, $\vec{A}\times\vec{B}$), i.e.,

$$\vec{k} = \vec{A}a + \vec{B}b + \vec{A}\times\vec{B}c, \quad (10)$$

or in a matrix form as

$$\begin{bmatrix} k_1 \\ k_2 \\ k_3 \end{bmatrix} = \left[\vec{A}, \vec{B}, \vec{A} \times \vec{B} \right] \begin{bmatrix} a \\ b \\ c \end{bmatrix}, \tag{11}$$

where a, b and c are the combination coefficients. For a $\vec{k}$ given in Equation 8, we have $a = \cos^2\theta$, $b = \sin^2\theta$ and $c = 0$, which are functions of θ. In experiments, on the other hand, the measured quantities are the change rates of Raman shifts ($\vec{k}$). With Equation 11, it is straightforward to calculate a and b from the measured $\vec{k}$:

$$\begin{cases} a = 0.0129k_1 - 0.088k_2 - 0.0491k_3 \\ b = -0.2785k_1 + 0.0104k_2 + 0.0557k_3 \end{cases}, \tag{12}$$

and further estimate θ from them:

$$\theta = \begin{cases} 0° & (\text{if } a < 0) \\ 90° & (\text{if } b < 0) \\ \arccos\sqrt{\dfrac{a}{a+b}} & (\text{if } a > 0 \text{ and } b > 0) \end{cases}. \tag{13}$$

Here, we determine θ from the changes of all three modes, but not merely from one mode. This effectively reduces the error caused by experimental uncertainty as will be demonstrated below.

To test the validity of the proposed method in detecting BP orientation, we conducted Raman experiments on a series of BP samples under different uniaxial strain. The BP flakes of different thicknesses were mechanically exfoliated from bulk BP crystals onto the flexible polyethylene terephthalate (PET) substrate, the optical images are shown in **Figure 3**a-c. By stretching the substrate along certain direction (blue arrows shown in Figure 3a-c), uniaxial strain was introduced into the BP samples controllably and uniformly. In our cases, the uniaxial strain was applied along three directions, that is, θ=0° (ZZ), θ=30° and θ=90° (AC). Angle-dependent polarized Raman spectroscopy before applying strain was used to directly

determine the crystalline orientation of BP flakes in experiments, more details can be seen in the Supporting Information (Figure S6). The Raman measurement results are summarized in Figure 3d-i. It is clearly seen that the Raman peak positions change with the applied strain (Figure 3d-f). The fitted frequencies as a function of strain are plotted in Figure 3h-j, and the obtained change rates k_1, k_2 and k_3, as well as the resulting *a*, *b* and θ from Equation 12 and Equation 13, are listed in **Table 1**. The θ determined from the proposed method are 0°, 33.3° and 90° for three samples, respectively, agreeing well with the direct measurements (0°, 30° and 90°).

We further test the proposed method using reported experimental data of Raman shifts under different strains. The sets of change rates (k_1, k_2, k_3) in **Table 2** are extracted from literatures.[24,25] Samples #4–#6 (BP on PET) were measured using 532 nm laser excitation, and was simplified as "spread BP@PET" in the following. Samples #7-#8 were performed under 488 nm, the ultrathin BP is sandwiched by the top polymethyl methacrylate (PMMA) layer and the bottom PET substrate, which was named as "sandwiched PMMA@BP@PET". The thickness of BP samples were within 50 nm for stretching. Samples #9, #10, #9$^{\beta}$ and #10$^{\beta}$ are simulated values by Li et al.,[24] where a Poisson's ratio of PET (0.33) was used for #9$^{\beta}$ and #10$^{\beta}$. The θ values determined from the (k_1, k_2, k_3) data with on our proposed method are in good agreement with reported values, with the average discrepancy being as small as 3.2°. This further confirms the validity and universality of the proposed method, which does not rely on the excitation wavelength, sample thickness and substrates.

The proposed method is built on the overall relative changes of three characteristic Raman modes instead of one absolute value, which is conductive to better accuracy under experimental uncertainties. The data in Table 1 and Table 2 show that the absolute values of change rates by "spread BP@PET" experiment (sample #1-#6) are smaller than those by "sandwiched PMMA@BP@PET" set-ups and simulated results (sample #7-#10) on the whole.

The most notable case is the Raman shift rates of B_{2g} mode: the absolute rates by sandwiched stacking in sample #7 and #8 are more than three times those by spread structure in sample #1 and #3 even when the strain are applied in identical direction. Therefore, the criterion for identifying the orientation by the absolute change of one particular vibrational mode may be not suitable for distinct experimental configurations.[24,25] Our proposed method is able to compensate the error caused by the absolute measurements in different conditions.

2.3. Calculation of the effective strain applied in BP

In practice, strain is applied directly upon the substrate and then transduces to the supported 2D sheet such as BP. Rigorously speaking, what is measured in experiments is the strain in substrate, but not that of 2D sheet. Due to the difference of elastic constants (including Poisson's ratio) between the substrate and 2D sheet and the weak interaction between them, slippage at the interface between the 2D sheet and the substrate likely happens during stretching, leads to the low efficiency of applied strain and the overestimation of the strain in the 2D sheet material. As a result, the deviation of measured physical properties would be observed.[24,25,28] Therefore, the estimation of the effective strain is important, which still remains elusive. Based on the results above, here we develop a scheme to estimate the effective strain in 2D sheet.

Under ideal situations, the applied efficiency of strain can be estimated from any Raman mode of BP flakes as the ratio of experimental to calculated change rates under a uniaxial strain:

$$\eta_i = \frac{k_i(\text{Expt.})}{k_i(\text{Calc.})}, i = 1,2,3 \tag{14}$$

where $k_i(\text{Expt.})$ are measured values in experiments, and $k_i(\text{Calc.})$ are the back-calculated values with Equation 8 using a θ value determined from $k_i(\text{Expt.})$ as explained in the

previous section. For practical case, data uncertainty is unavoidable, so we calculate the strain efficiency as the weighted average of η_i:

$$\bar{\eta} = \frac{\sum_{i=1}^{3} \eta_i |k_i(\text{Calc.})|}{\sum_{i=1}^{3} |k_i(\text{Calc.})|}. \quad (15)$$

The approach was applied to analyze different samples and the results are summarized in **Table 3**. For the widely used "spread BP@PET" strain transfer set-ups, only 20% to 40% of strain is transferred to BP flakes effectively from PET substrates. For the improved "sandwiched PMMA@BP@PET" experimental assembly, the strain can be viewed as being transferred to BP samples completely. It is also noted that in Table3, almost all the absolute rates in calculation are larger than, or at best close to experimental measurements expect the B_{2g} mode in the sandwiched system of #7 and #8. For B_{2g} mode, the atomic displacement is mainly along the ZZ direction (see Figure 1c), which is changed weakly when being strained along AC direction in theoretical calculations,[24,25,29] but the experimental value (–1.85) is three times larger than expectation (–0.68) for sample #8. The same discrepancy is also observed in the literature,[25] and this is mainly responsible for the mismatch angle of the sample #8 in Table 2 and the abnormal 124% strain efficiency in Table 3.

2.4. Simplified model for the determination of angle θ

As stated above, θ of BP samples can be determined from the change rates (k_1, k_2, k_3) of the three characteristic Raman shifts according to Equation 12 and Equation 13, where (k_1, k_2, k_3) were fitted from a series of data points with different strain amplitude. Actually, as we have discussed, the strain may be not applied to BP effectively in experiments. However, our method is not directly related to absolutely applied strain, but only depends on the relative changes of three characteristic Raman shifts. Therefore, (k_1, k_2, k_3) can be replaced by the changes of Raman shifts $(\Delta\omega_1, \Delta\omega_2, \Delta\omega_3)$ under two different strain amplitudes, regardless of

the actual value ofthem. Taking the sample #2 as example, three groups of points under distinct strain in Figure 3h are selected, various frequency changes $(\Delta\omega_1, \Delta\omega_2, \Delta\omega_3)$ are analyzed in **Table 4**. Replacing the (k_1, k_2, k_3) in Equation 12 with $(\Delta\omega_1, \Delta\omega_2, \Delta\omega_3)$, θ was determined. It is shown that the accuracy of θ in this simplified scheme is acceptable. Therefore, the method is only related to the frequency changes under a distinct strain, and it even does not matter whether the initial state is unstrained or not.

Another issue to be noted is the sign of θ, which is positive or negative. Three characteristic Raman bands of BP samples can be observed under the typical backscattering geometry, with the measured frequencies denoted as ω_1, ω_2 and ω_3. After applying an in-plane arbitrary uniaxial strain, the frequencies move to ω_1', ω_2' and ω_3'. The changes of frequencies are $\Delta\omega_1 = \omega_1' - \omega_1$, $\Delta\omega_2 = \omega_2' - \omega_2$ and $\Delta\omega_3 = \omega_3' - \omega_3$. According to our method, the strain angle θ can be determined by the frequency changes under strain $\theta = f(\Delta\omega_1, \Delta\omega_2, \Delta\omega_3)$ as Equation 12 and Equation 13. However, since $\cos(-\theta) = \cos(\theta)$, the sign of θ is undetermined in this approach. As shown in **Figure 4**, the strain axis may locate in the clockwise (negative θ) or counterclockwise (positive θ) direction relative to the ZZ axis of BP sample. To determine the sigh of θ that is necessary for the complete determination of crystalline orientation, we propose to rotate the strain axis 45° counterclockwise on the basis of the previous strain direction and make an extra measurement. Denoted the resulting Raman shifts as ω_1'', ω_2'' and ω_3'', we can calculate $\Delta\omega_1' = \omega_1'' - \omega_1$, $\Delta\omega_2' = \omega_2'' - \omega_2$ and $\Delta\omega_3' = \omega_3'' - \omega_3$, and obtain a new angle: $\theta' = f(\Delta\omega_1', \Delta\omega_2', \Delta\omega_3')$. If θ' is larger than 45°, the original θ is positive; or if θ' is less than 45°, θ is negative. Based on the scheme, crystalline axes of BP structures can be determined completely.

3. Conclusion

In summary, an effective method is developed for identifying the crystalline orientation of BP samples by strain-induced Raman shifts, and it proved to be suitable for different experimental conditions. The evolutions of Raman spectra versus the gradually increased strain along ZZ, 30° and AC directions were studied experimentally, and the determined angles with the proposed method were in good agreement with those in the polarized Raman method. Different excitation wavelengths, sample thicknesses and substrates in distinct experimental conditions made little influence on the determination of crystalline orientation for stretchable BP flakes, further proving the universality of the method. Furthermore, an approach was developed to estimate the efficiency of applied strain for different BP samples, suggesting that only 20% to 40% strain were transferred to BP flakes effectively from PET substrates for "spread BP@PET" set-ups. This is instructive and meaningful to the study the stain related properties of BP as well as other layered materials. Our method gives better understanding to the strain effects on Raman shifts of BP, and its generalization to other 2D crystals is straightforward.

4. Calculation Methods and Experimental Section

Calculation Methods. All calculations were carried out by DFT using the QUANTUM ESPRESSO package.[30] The generalized gradient approximation with the Perdew-Burke-Ernzerhof (PBE) method is adopted to deal with exchange correlation functional.[31] The van der Waals (vdW) interactions were considered by the DFT-D2 approach of Grimme (denoted as PBE+D2),[32] and vdW density functional methods optB88-vdW (denoted as PBE+B88) and optB86b-vdW (denoted as PBE+B86b)[33] in the calculations of lattice parameters and optical phonon frequencies. See the Supporting Information for detailed results and analysis. For monolayer BP, at least 10 Å gaps between layers were set to eliminate the possible interactions. The Brillouin zones were sampled on an $8\times8\times10$ Monkhorst-Pack grid[34] for

bulk BP and 14×1×10 grid for monolayer BP. The structures were relaxed until all components of forces were less than 0.001 Ry $Bohr^{-1}$. The plane wave cutoff was set to 80 Ry for wave functions and 320 Ry for charge density within a norm-conserving pseudopotential. According to the analysis and comparison in the Supporting Information, the PBE functional was selected to calculate the Raman shifts under strain with a scaling factor of 1.04.

Fabrication and Characterization of Encapsulated BP flakes. Stretchable BP thin flakes used in this work were mechanically exfoliated from bulk BP crystals (Smart element) onto flexible polyethylene terephthalate (PET) substrate using Scotch tape. The uniaxial strain is applied on the PET substrate with BP sample through a home-built setup. Thin BP flakes were identified using an optical microscope (Olympus BX 51) to confirm it is suitable for further study. Strained Raman measurements were performed after determining the crystalline orientation. All the Raman spectroscopy measurements were conducted on a JY Horiba HR800 Raman system with 514.5 nm (2.41 eV) line from an Ar+ laser. The intensity of the laser was less than 100 μW to avoid damaging the BP samples.

Supporting Information

Supporting Information is available from the Wiley Online Library or from the author.

Acknowledgements
The work was supported by the National Natural Science Foundation of China (No. 21373015, 21233001, 21573004), the Ministry of Science and Technology (No. 2016YFA0200101, 2016YFA0200104 and 2015CB932400) and the China Postdoctoral Science Foundation (2015M580010).

Received: ((will be filled in by the editorial staff))
Revised: ((will be filled in by the editorial staff))
Published online: ((will be filled in by the editorial staff))

References

[1] H. O. Churchill,P. Jarillo-Herrero, *Nat. Nanotechnol.* **2014,** *9*, 330.

[2] P. W. Bridgman, *J. Am. Chem. Soc.* **1914,** *36*, 1344.

[3] J. Qiao,X. Kong,Z. X. Hu,F. Yang,W. Ji, *Nat. Commun.* **2014,** *5*, 4475.

[4] V. Tran,R. Soklaski,Y. Liang,L. Yang, *Phys. Rev. B* **2014,** *89*, 235319.

[5] A. Morita, *Appl. Phys. A* **1986,** *39*, 227.

[6] L. Li,Y. Yu,G. J. Ye,Q. Ge,X. Ou,H. Wu,D. Feng,X. H. Chen,Y. Zhang, *Nat. Nanotechnol.* **2014,** *9*, 372.

[7] A. Castellanos-Gomez,L. Vicarelli,E. Prada,J. O. Island,K. L. Narasimha-Acharya,S. I. Blanter,D. J. Groenendijk,M. Buscema,G. A. Steele,J. V. Alvarez,H. W. Zandbergen,J. J. Palacios,H. S. J. van der Zant, *2D Materials* **2014,** *1*, 025001.

[8] J. Qiao,X. Kong,Z. X. Hu,F. Yang,W. Ji, *Nat. Commun.* **2014,** *5*, 5475.

[9] X. Ling,H. Wang,S. Huang,F. Xia,M. S. Dresselhaus, *Proc. Natl. Acad. Sci. U.S.A.* **2015,** *112*, 4523.

[10] J. W. Jiang,H. S. Park, *Nat. Commun.* **2014,** *5*, 4727.

[11] F. Xia,H. Wang,Y. Jia, *Nat. Commun.* **2014,** *5*, 5458.

[12] H. Lang,S. Zhang,Z. Liu, *Phys. Rev. B* **2016,** *94*, 235306.

[13] X. Ling,S. Huang,E. H. Hasdeo,L. Liang,W. M. Parkin,Y. Tatsumi,A. R. Nugraha,A. A. Puretzky,P. M. Das,B. G. Sumpter,D. B. Geohegan,J. Kong,R. Saito,M. Drndic,V. Meunier,M. S. Dresselhaus, *Nano Lett.* **2016,** *16*, 2260.

[14] J. W. Jiang, *Nanotechnology* **2015,** *26*, 055701.

[15] A. C. Ferrari,D. M. Basko, *Nat. Nanotechnol.* **2013,** *8*, 235.

[16] Y. Feng,W. Zhou,Y. Wang,J. Zhou,E. Liu,Y. Fu,Z. Ni,X. Wu,H. Yuan,F. Miao,B. Wang,X. Wan,D. Xing, *Phys. Rev. B* **2015,** *92*, 054110.

[17] J. Wang,S. Zhang,J. Zhou,R. Liu,R. Du,H. Xu,Z. Liu,J. Zhang,Z. Liu, *Phys. Chem. Chem. Phys.* **2014,** *16*, 11303.

[18] J. Wu,N. Mao,L. Xie,H. Xu,J. Zhang, *Angew. Chem. Int. Ed.* **2015,** *54*, 2366.

[19] H. B. Ribeiro,M. A. Pimenta,C. J. de Matos,R. L. Moreira,A. S. Rodin,J. D. Zapata,E. A. de Souza,A. H. Castro Neto, *ACS Nano* **2015,** *9*, 4270.

[20] W. Lu,X. Ma,Z. Fei,J. Zhou,Z. Zhang,C. Jin,Z. Zhang, *Appl. Phys. Lett.* **2015,** *107*, 021906.

[21] J. Kim,J. U. Lee,J. Lee,H. J. Park,Z. Lee,C. Lee,H. Cheong, *Nanoscale* **2015,** *7*, 18708.

[22] N. N. Mao,J. X. Wu,B. W. Han,J. J. Lin,L. M. Tong,J. Zhang, *Small* **2016,** *12*, 2627.

[23] X. Ling,L. Liang,S. Huang,A. A. Puretzky,D. B. Geohegan,B. G. Sumpter,J. Kong,V. Meunier,M. S. Dresselhaus, *Nano Lett.* **2015,** *15*, 4080.

[24] Y. Wang,C. Cong,R. Fei,W. Yang,Y. Chen,B. Cao,L. Yang,T. Yu, *Nano Research.* **2015,** *8*, 3944.

[25] Y. Li,Z. Hu,S. Lin,S. K. Lai,W. Ji,S. P. Lau, *Adv. Funct. Mater.* **2016**, DOI: 10.1002/adfm.201600986.

[26] M. Huang,H. Yan,C. Chen,D. Song,T. F. Heinz,J. Hone, *Proc. Natl. Acad. Sci. U.S.A.* **2009,** *106*, 7304.

[27] C. Rice,R. J. Young,R. Zan,U. Bangert,D. Wolverson,T. Georgiou,R. Jalil,K. S. Novoselov, *Phys. Rev. B* **2013,** *87*, 081307.

[28] S. Zhang,J. Wang,Z. Li,R. Zhao,L. Tong,Z. Liu,J. Zhang,Z. Liu, *J. Phys. Chem. C* **2016,** *120*, 10605.

[29] R. Fei,L. Yang, *Appl. Phys. Lett.* **2014,** *105*, 083120.

[30] P. Giannozzi, *J. Phys.: Condens. Matter* **2009,** *21*, 395502.

[31] J. P. Perdew,K. Burke,M. Ernzerhof, *Phys. Rev. Lett.* **1996,** *77*, 3865.

[32] S. Grimme, *J. Comput. Chem.* **2006,** *27*, 1787.

[33] M. Dion,H. Rydberg,E. Schroder,D. C. Langreth,B. I. Lundqvist, *Phys. Rev. Lett.* **2004,** *92*, 246401.

[34] H. J. Monkhorst,J. D. Pack, *Phys. Rev. B* **1976,** *13*, 5188.

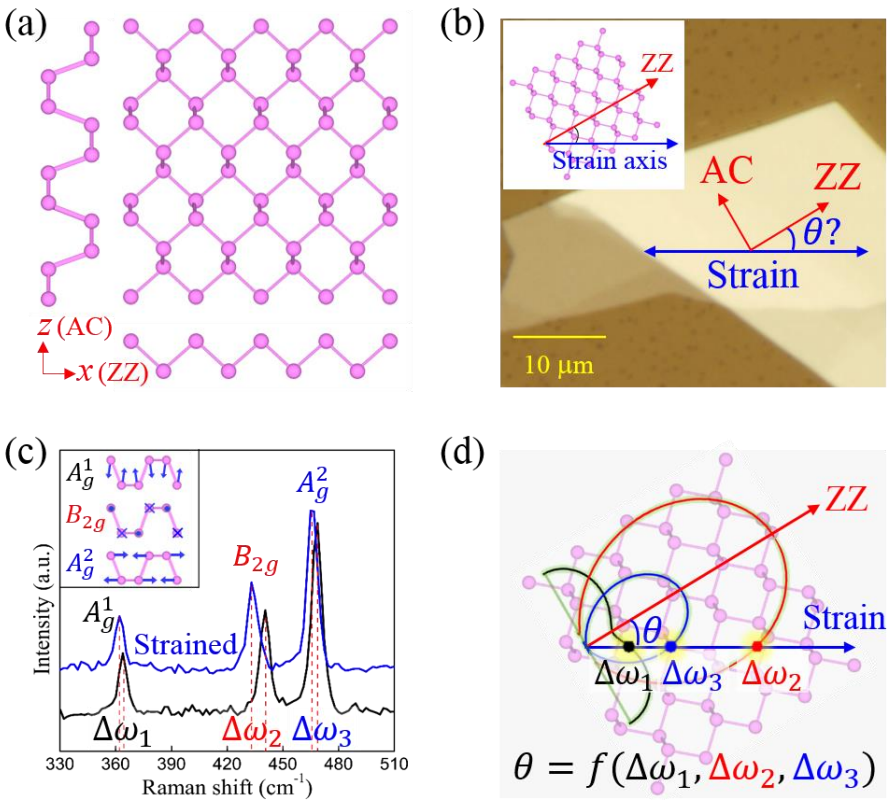

Figure 1. The sketch of how the crystalline orientation of BP can be determined from the shift patterns of Raman bands under a uniaxial strain. a) Geometrical structure of monolayer BP. The *x* and *z* axes are along zigzag (ZZ) and armchair (AC) directions, respectively, following the conventional notation in bulk BP. b) Optical micrograph of BP flake, the angle θ between uniaxial strain and ZZ direction is indicated. c) The corresponding Raman spectra of strained (blue band) and unstrained (black band) BP flake in panel (b) under backscattering configurations. Inset shows the atomic displacements for the three characteristic Raman modes. d) The changes of Raman shifts $(\Delta\omega_1, \Delta\omega_2, \Delta\omega_3)$ under strain have different dependences on θ, and θ can be back calculated from the measured pattern of $(\Delta\omega_1, \Delta\omega_2, \Delta\omega_3)$.

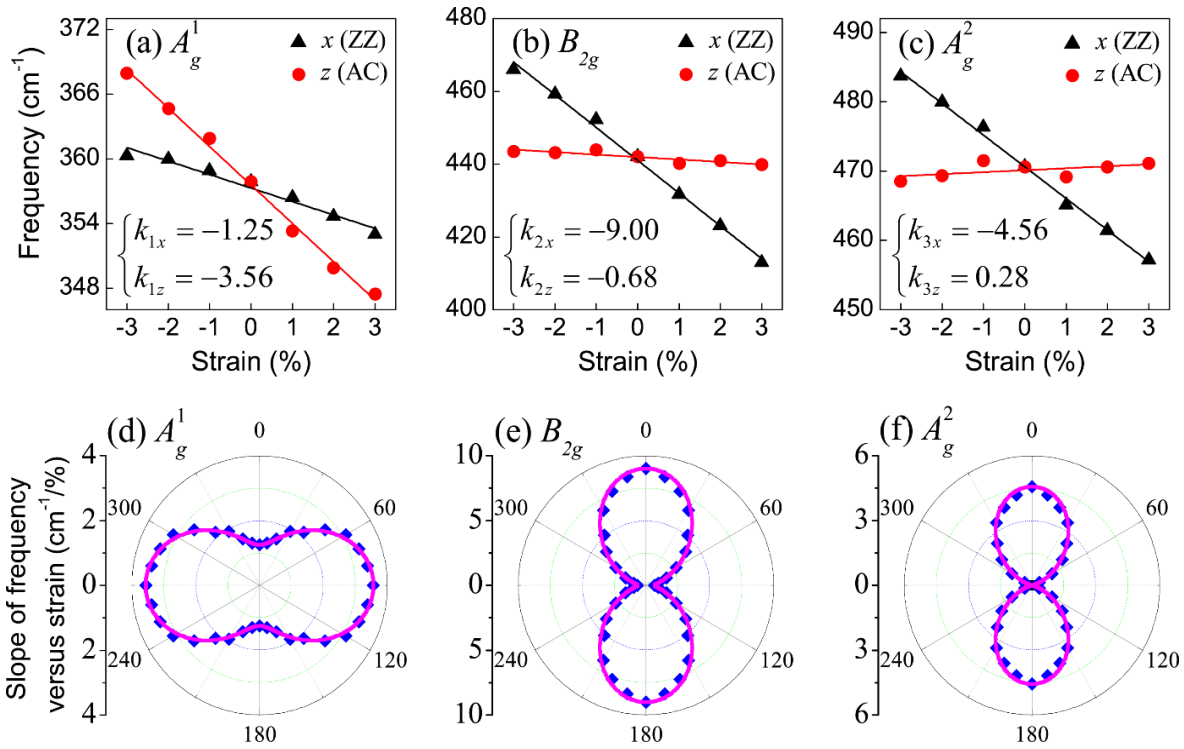

Figure 2. The change of Raman shifts under uniaxial strain. a-c) Raman shifts versus uniaxial strain along x (ZZ) direction (black triangle) and z (AC) direction (red dot) of A_g^1, B_{2g} and A_g^2 modes of monolayer BP. k_x and k_z (in units of cm^{-1}/%) are the change rates of frequency under these two typical directions. d-f) The corresponding θ-dependent change. The solid curves are calculated with Equation 7 with k_x and k_z determined in (a-c), and the scattering points are obtained with direct DFT calculations at each θ.

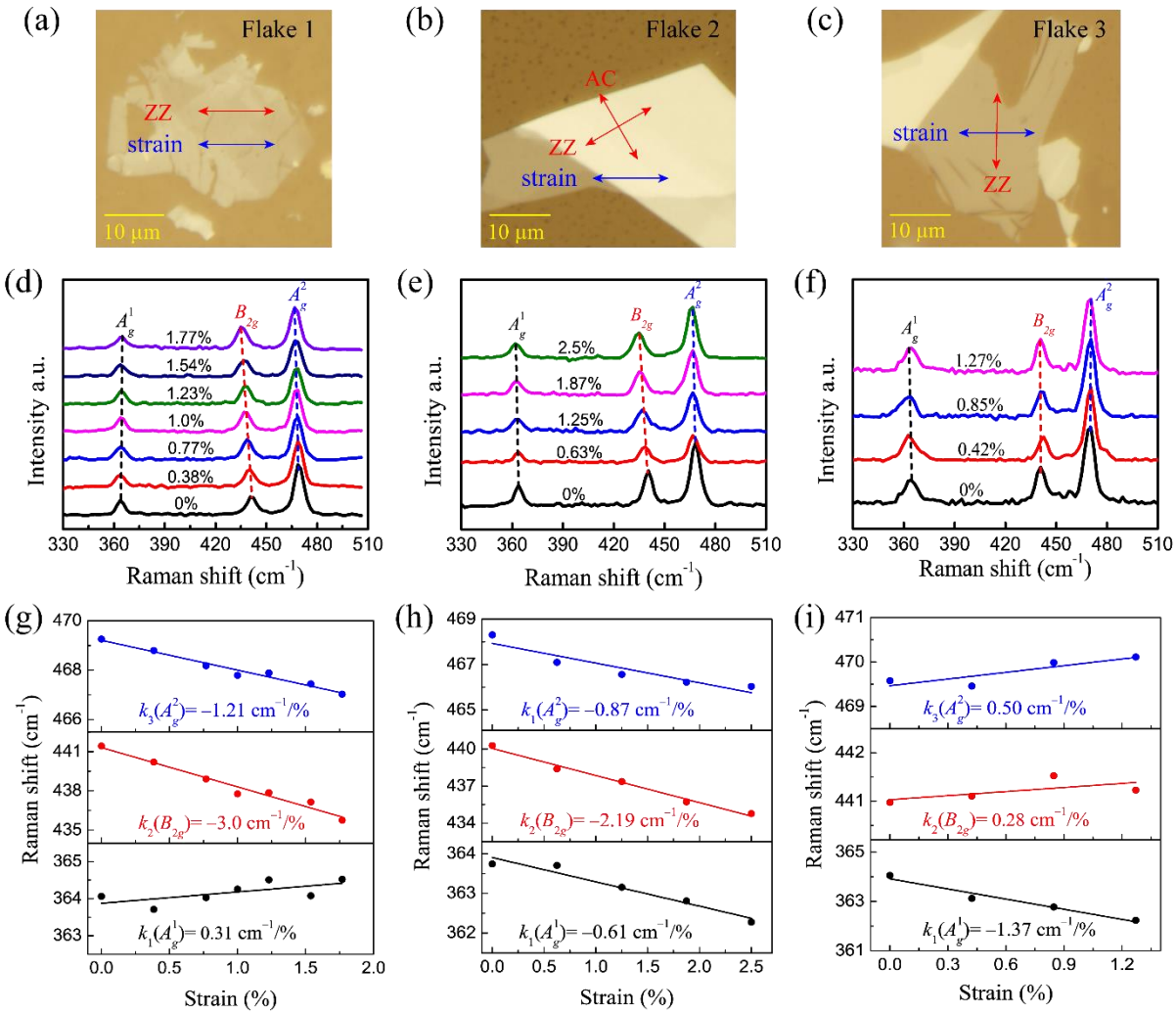

Figure 3. Determination of BP orientation from the change of Raman shifts under a uniaxial strain. a-c) Optical micrograph of the encapsulated BP flakes on PET substrate. The uniaxial strain is applied at different angles: (a) θ =0°, (b) θ =30° and (c) θ =90°. d-f) The Raman spectra of BP as the applied strain increased gradually for the corresponding samples in Figure 3a-c under 514.5 nm excitation. g-i) The corresponding fitted Raman shifts as a function of applied strain for the three BP flakes.

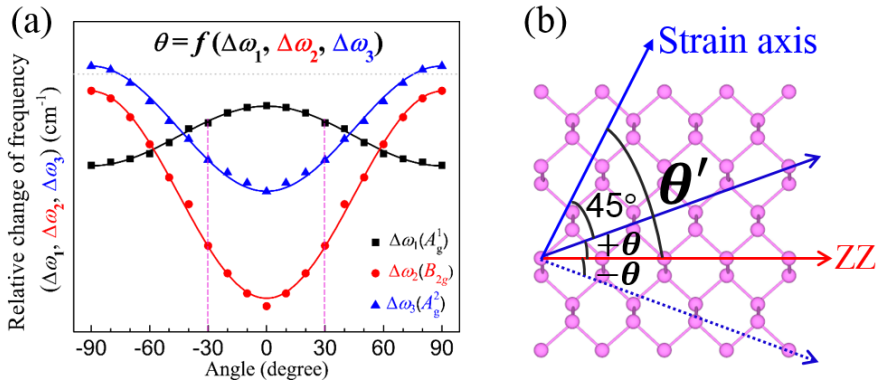

Figure 4. The direction of strain relative to ZZ axis of BP. a) Changes of the three characteristic Raman modes as a function of strain angle with certain magnitude. b) The relative angle of strain axis respect to ZZ direction of monolayer BP lattice. The blue solid

arrow with positive angle mean strain in the counterclockwise direction, and the dotted arrow with negative angle means strain in clockwise direction.

Table 1. The experimental determination of BP orientation with the proposed method using the change rates (k_1, k_2, k_3) (in units of cm^{-1}/% strain) of Raman shifts under a uniaxial strain.

Sample #	$k_1(A_g^1)$	$k_2(B_{2g})$	$k_3(A_g^2)$	a	b	Angle θ (degree)	
						Direct measurement[a)]	Proposed method[b)]
1	0.31	-3.0	-1.21	0.33	-0.18	0	0
2	-0.61	-2.19	-0.87	0.23	0.10	30	33.3
3	-1.37	0.28	0.5	-0.07	0.41	90	90

[a)] Determined by angle-dependent polarized Raman spectroscopy.
[b)] Determined with the proposed Equation 12 and Equation 13 by measuring Raman shifts under strains.

Table 2. The determination of BP orientation based on the reported change rates (k_1, k_2, k_3) (in units of cm^{-1}/%).

	Sample #	$k_1(A_g^1)$	$k_2(B_{2g})$	$k_3(A_g^2)$	a	b	Angle θ (degree)	
							Refs.	Proposed method[a)]
Expt.[24]	4	-1.3	-0.25[α]	0.25[α]	0.018	0.347	75	77.1
	5	-0.31[α]	-2.3	-1.1	0.258	0.002	10	5.3
	6	-1.1	-1.4	-0.5	0.137	0.266	56	54.4
Expt.[25]	7	-0.52	-10.92	-4.32	1.192	-0.205	0	0
	8	-3.81	-1.85	-0.03	0.118	1.047	90	71.4
Sim.[25]	9	0.19	-9.27	-4.06	1.04	-0.373	0	0
	9[β]	1.12	-9.11	-4.1	1.018	-0.636	0	0
	10	-2.35	-0.7	0.52	0.006	0.680	90	84.4
	10[β]	-2.21	2.16	2.01	-0.317	0.750	90	90

[α]Data are fitted according to data in references.
[β]The values are simulated under Poisson's ratio of 0.33.
[a)] Determined with the proposed Equation 12 and Equation 13 from the reported (k_1, k_2, k_3).

Table 3. The experimental (Expt.) and calculated Raman shift rates ($\partial\omega/\partial\varepsilon$, cm^{-1}/% strain) of the three characteristic Raman modes and the efficiency of applied strain in experiments.

Sample #	θ (degree)		$k_1(A_g^1)$	$k_2(B_{2g})$	$k_3(A_g^2)$	Strain efficiency[a)]
1	0°	Expt.	0.31	-3.0	-1.21	26.33%
		Calc.	-1.25	-9.0	-4.56	
2	30°	Expt.	-0.61	-2.2	-0.87	30.4%
		Calc.	-1.83	-6.92	-3.35	
3	90°	Expt.	-1.37	0.28	0.5	35.2%
		Calc.	-3.56	-0.68	0.28	
4	75°	Expt.[24]	-1.3	-0.25	0.25	27.7%
		Calc.	-3.4	-1.24	-0.044	
5	10°	Expt.[24]	-0.31	-2.3	-1.1	27.5%
		Calc.	-1.32	-8.75	-4.41	

6	56°	Expt.[24]	-1.1	-1.4	-0.5	40.8%
		Calc.	-2.84	-3.28	-1.23	
7	0°	Expt.[25]	-0.52	-10.9	-4.32	106%
		Calc.	-1.25	-9.0	-4.56	
8	90°	Expt.[25]	-3.81	-1.85	-0.03	124%
		Calc.	-3.56	-0.68	0.28	

[a)] Determined with Equation 15.

Supporting Information

In-plane uniaxial strain in black phosphorus enables the identification of crystalline orientation

Shuqing Zhang, Nannan Mao, Juanxia Wu, Lianming Tong, Jin Zhang,* and Zhirong Liu**

In this supporting information, we combine the qualitative analysis by group theory with quantitative calculation using density functional theory (DFT) make helpful explorations to some unsolved problems of bulk BP and monolayer BP.

S1. The structure of BP is analyzed from the view of symmetry and the lattice parameters are calculated by different functionals.

S2. The frequencies of optical phonon modes are calculated and analyzed.

S3. A standardized **k**-path form was adopted to calculate the band structure and phonon dispersion of bulk and monolayer BP.

S4. The change rates of optical phonon frequencies versus uniaxial strain are shown. S5. Polarized Raman spectroscopy with consideration of the effects of excitation wavelength and sample thickness, is used to determine the crystalline orientation of BP flakes in experiments.

S1. Lattice parameters and structure symmetry analysis

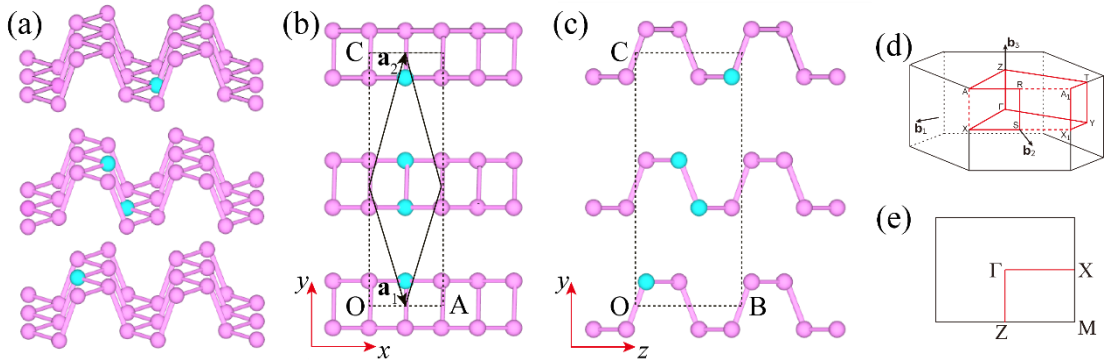

Figure S1. Crystalline structure of bulk BP, represented in (a) perspective view, (b) right view and (c) front view. The conventional cell is shown by the dotted rectangle and primitive cell in solid rhombus. The primitive cell consists of four blue atoms. Monolayer BP is the case with single puckered layer in *y* direction. (d-e) The first Brillouin zone for bulk (d) and single-layer black phosphorus (e).

As shown in Figure S1, the conventional unit cell of bulk BP belongs to primitive orthorhombic Bravais lattice, the experimental lattice constants a=OA=3.31 Å, b=OC=10.5 Å and c=OB= 4.38 Å.[1] There are eight atoms in the conventional cell and it is not the smallest possible group for bulk BP. The orthorhombic crystal system with one additional point at the center of one face (bottom) in the cell forms base-centered orthorhombic Bravais lattice, which is the lattice structure of the primitive cell of bulk BP, as shown in Figure S1 (b) with solid rhombus. The primitive lattice can be written as

$$\begin{cases} \mathbf{a}_1 = (a/2, -b/2, 0) \\ \mathbf{a}_2 = (a/2, b/2, 0) \\ \mathbf{a}_3 = (0, 0, c) \end{cases} . \quad (1)$$

For base-centered lattice, the base are viewed as the *xy*-plane in the crystal coordinate system (*xyz*), so the direction along *y* is defined perpendicular to layers in bulk BP in general descriptions, rather than *z* in other similar layered materials such as graphite or transition metal dichalcogenides. The reciprocal lattice for bulk BP have a reciprocal relationship with the base-centered orthorhombic Bravais lattice in real space. The relationship of unit vectors between real space and reciprocal space is

$$\mathbf{a}_i \cdot \mathbf{b}_j = 2\pi\delta_{ij} \quad (2)$$

so the reciprocal vectors can be written as

$$\begin{cases} \mathbf{b}_1 = (2\pi/a, -2\pi/b, 0) \\ \mathbf{b}_2 = (2\pi/a, 2\pi/b, 0) \\ \mathbf{b}_3 = (0, 0, 2\pi/c) \end{cases} \quad (3)$$

The first Brillouin zone in reciprocal space is shown in Figure S1 (d) with vectors $\mathbf{b}_1$, $\mathbf{b}_2$, $\mathbf{b}_3$ and special **k**-vector points Γ, X, S, R, A, Z, Y, X_1, A_1, T.

For monolayer BP in 2D system, the symmetry properties in the direction perpendicular to the plane are no longer working, it also means there is no centered point in the *xy*-plane, so the conventional cell and primitive cell of 2D BP are only simple rectangle. The first Brillouin zone is also a rectangular, the corresponding high-symmetry points are shown in Figure S1(e). The armchair direction of two dimensional system also set as z axis for the conformity with bulk phase.

The numerical lattice parameters by different methods as well as the experimental results are listed in Table S1. We find that the PBE+optB86b functional produce the most consistent lattice geometry with experiments, especially the interlayer spacing constant, as shown in other literatures.[2,3] The pure PBE and PBE+B88 with vdW correction give close results in the plane as well. For the moment, the fabrication of monolayer phosphorus is mainly driven

by mechanical cleavage, the lattice constants should not change a lot, and the calculations also think so. The constants of bulk and monolayer BP are distinguished by an oblique line in Table S1. Theoretically, the layer spacing of single layer BP ought to be infinity, dashes are used in the table.

Table S1. The relaxed lattice parameters of bulk BP and monolayer (1L) BP with PBE, PBE+D2, PBE+B88 and PBE+B86b.

		a	b	c
Bulk/1L BP	PBE	3.30/3.29	11.32/–	4.55/4.61
	PBE+D2	3.36/3.35	11.33/–	4.73/4.77
	PBE+B88	3.33/3.31	10.74/–	4.48/4.58
	PBE+B86b	3.33/3.30	10.54/–	4.36/4.51
	Expt.	3.31	10.50	4.38

S2. Optical phonon modes

As stated above, *y* axis is defined perpendicular to layers in bulk BP because of its base-centered orthorhombic Bravais lattice. The setting of crystal coordinate system plays an important role in assigning the vibrational modes of Raman and infrared frequencies, it also essential for the experimental configurations of polarized Raman scattering.

According to the fundamental Raman and infrared selection rules, only the optical phonons near the center point Γ (q≈0) of Brillouin zone are active. What may cause confusion is that the symmetry assignment of vibrational frequencies are different in literatures, the modes at ~230 cm^{-1} and ~470 cm^{-1} are characterized as B_{3g}^1 and B_{2u} in some articles,[4-6] but as B_{2g}^2 and B_{3u} respectively by others.[7-9] All of these stem from the different set of coordinate axis of crystal. We should note that Raman tensors are in certain coordinate system, if it is inconsistent with calculation or experimental coordinates, which may cause conflicts in assigning vibrational frequencies. Obviously, some papers have not noticed it, the Raman tensor in the first system was used, but their crystal coordinates are built in the second way.[10,11] However, consistent coordinate system is crucial important for detecting different vibrational modes with appreciate scattering configurations in polarization Raman measurements.[12]

As for the calculations of vibrational frequencies, which are generally studied under the harmonic approximation, it is the biggest reason for disagreements between calculations and experiments. For now, the most common way of compensating the anharmonic effect is to multiply by scaling factors.[13] The optical phonon frequencies of bulk and monolayer BP by

PBE, PBE+D2, PBE+B88 and PBE+B86b functionals are shown in Table S2, and they are respectively rescaled by 1.04, 1.12, 1.07 and 1.06 to make better comparison with experimental data. Balancing the complexity and accuracy of calculations, the PBE fuctional with a scaling factor 1.04 is selected to calculate Raman shifts in the main text.

The atomic displacements of optical phonon modes at the center of Brillouin zone in bulk BP are shown in Figure S2. Monolayer BP is the case of single puckered layer.

Table S2. The optical phonon frequencies (in units of cm^{-1}) of bulk and monolayer BP by different calculation methods and experiments.

	Bulk frequency					Monolayer frequency				
Symmetry	Expt.[5]	PBE	PBE+D2	PBE+B88	PBE+B86b	Expt.[14]	PBE	PBE+D2	PBE+B88	PBE+B86b
B_{1u}	136	137.3	137.3	138.4	111.2		144.2	168.7	149.2	140.3
B_{1g}	197	194.9	194.9	200.6	195.3		196.1	202.7	203.2	202.2
A_g^1	365	353.1	326.6	355.7	361.8	363	357.7	332.0	359.7	366.3
B_{3g}^1	233	232.5	232.5	232.4	229.5		233.2	226.8	235.3	234.7
A_u		432.0	432.0	426.0	428.4		433.6	418.8	432.7	432.3
B_{2g}	440	441.1	441.1	438.1	437.8	440	442.0	451.4	441.8	439.8
B_{3g}^2	442	439.4	439.4	437.3	430.4		444.0	434.9	446.6	445.4
A_g^2	468	469.2	469.0	468.7	467.3	471	470.5	473.7	471.8	468.7
B_{2u}	469	478.1	478.1	484.2	482.6		479.4	479.4	487.6	486.4

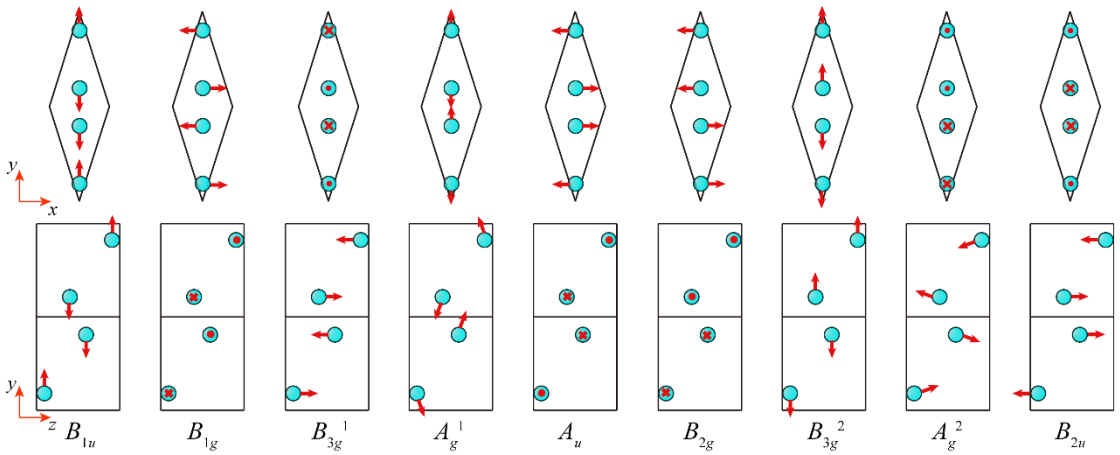

Figure S2. Atomic displacements of optical phonon modes at the center of Brillouin zone in bulk BP. The upper layer for the atomic motions in *xy*-plane, and the lower layer for corresponding view in *zy*-plane. The red arrows show the directions and amplitudes of motions, red dot represent outward movement, and opposite direction with cross.

S3. Band structure and phonon dispersion

Electronic band structure and phonon dispersion describe the energies of electrons and phonons respectively, they are the foundations for studying physical properties of crystals. Generally, the bands are plotted with the energy values $E_n(\mathbf{k})$ for wavevector **k** along a path of special high symmetry points in the Brillouin zone, and the path set usually called **k**-path, which is essential in the investigations of optical absorption, phonon transport and electron-phonon interaction.[2,15] Although the band and phonon structures of BP have calculated more than once in the literatures for the last two years,[2,16] they are distinct from each other in the **k**-path definition. A standardized **k**-path form was adopted as described in the reference,[17] which summarized authentic **k**-path sets for all the possible 14 Bravais lattices. This is beneficial to the extension and recycle in different project, and more importantly, it is more reliable. Band structures and phonon dispersions of bulk BP and monolayer BP by PBE fuctional are shown in Figure S3.

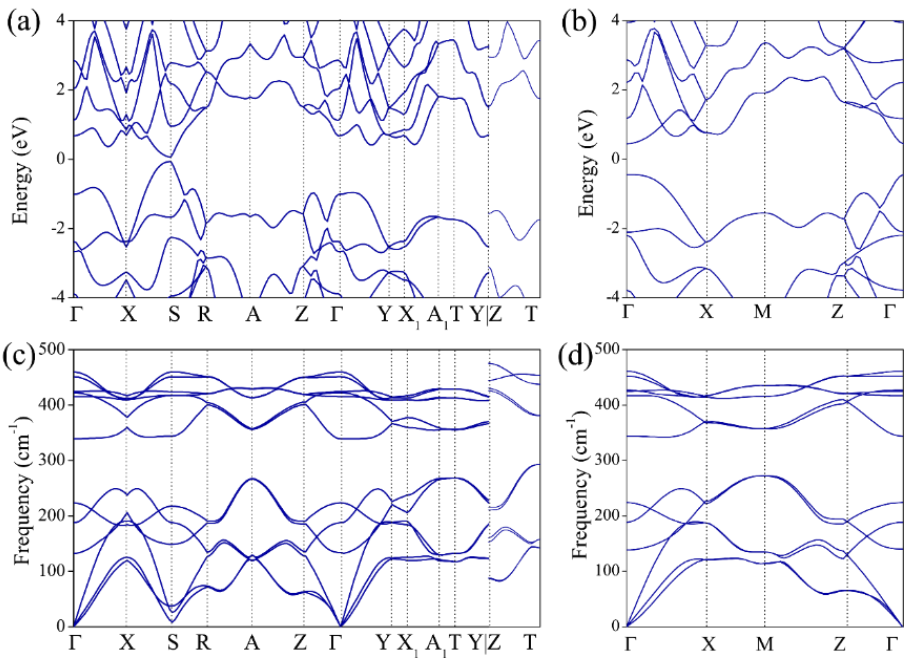

Figure S3. Band structure and phonon dispersion of (a), (c) bulk BP and (b), (d) monolayer BP, respectively. The lines are along the standardized high symmetry points.

S4. The frequency-to-strain rates of all the optical phonons

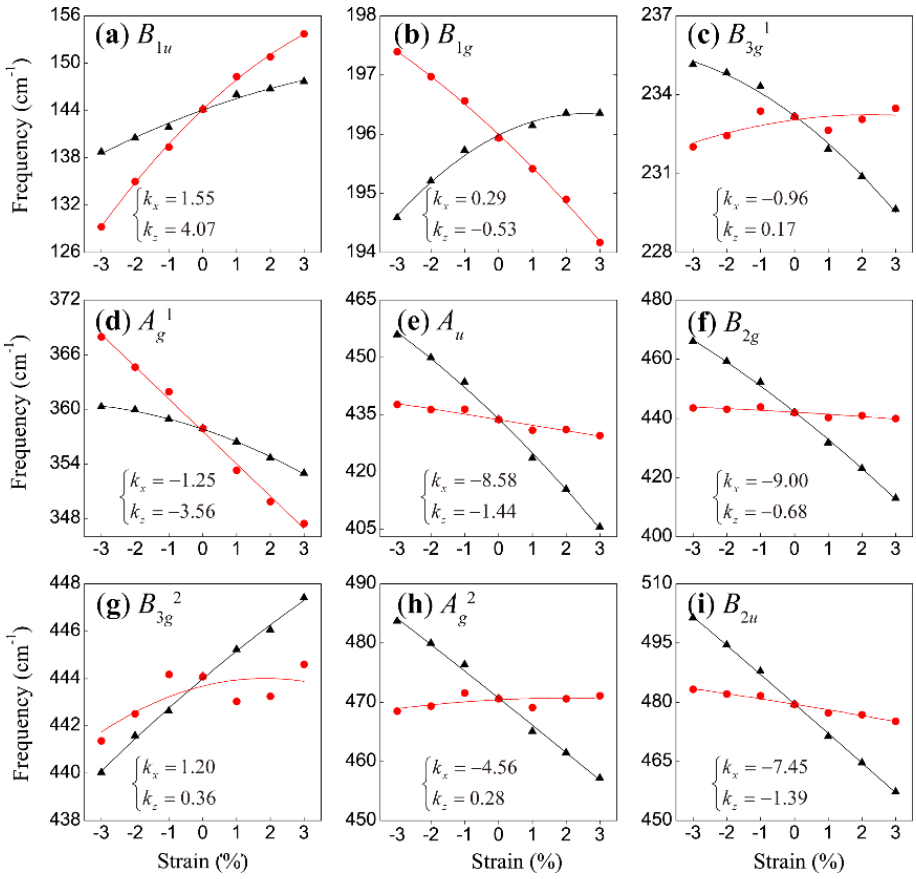

Figure S4. Raman shifts versus uniaxial strain along *x*-direction (black triangle) and *z*-direction (red dot) of all the optical phonon modes for monolayer BP. The k_x and k_z (in units of cm^{-1}/%) are slopes of frequency under two typical types of strain.

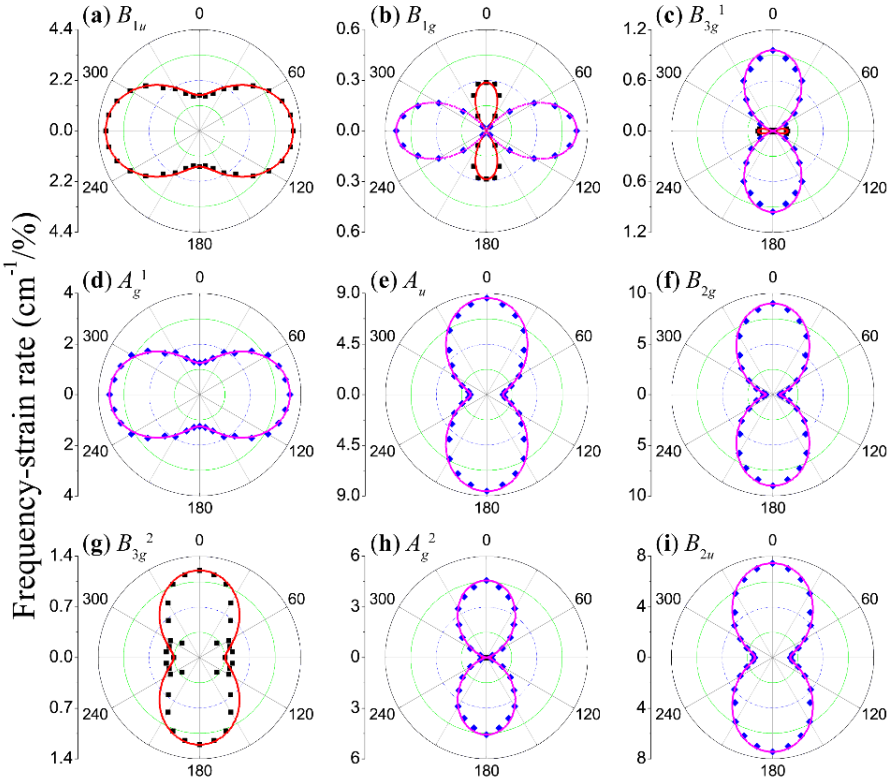

Figure S5. Angular dependence slopes of Raman shift versus strain for all the optical phonon modes of monolayer BP. The function curves in red and magenta lines are corresponding to positive and negative rates, respectively. The rate $\frac{\partial \omega}{\partial \varepsilon}$ for 10-degree interval are calculated directly by first principles theory, corresponding to points with black square and blue rhombus.

S5. Polarized Raman spectroscopy

The crystalline orientations of BP flakes are determined by angle-dependent polarized Raman spectroscopy with considering the optical effects of excitation wavelength and flake thickness. The thickness of BP flakes are thinner than 50 nm for better stretching in the experiments. The excitation wavelength of laser is 514.5 nm (2.41 eV). According to reported experiments and theoretical model,[15,18-20] for the configuration of thickness within 50 nm and exciting at 514.5 nm, the intensity of A_g^2 mode reach a maximum in the armchair crystallographic orientation under parallel polarization configurations. The strain are selectively applied to the zigzag, 30 degree and armchair directions, as discussed in the body.

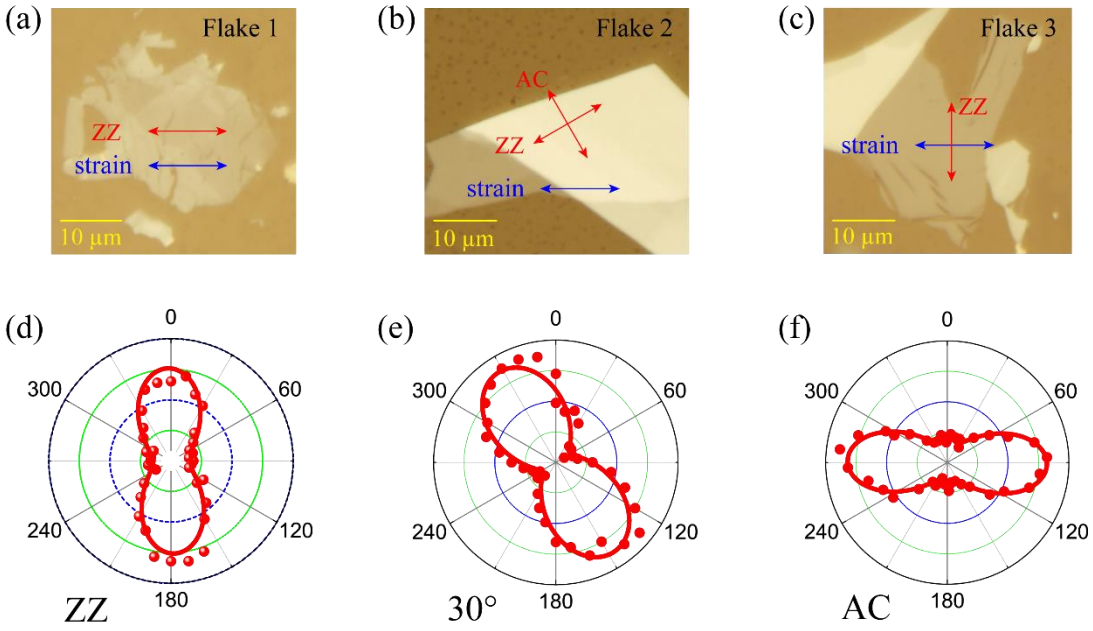

Figure S6. Optical micrograph of the exfoliated BP flakes on PET substrate, the uniaxial strain are applied along (a) θ=0°, (b) θ=30° and (c) θ=90°, respectively. (d-f) Polar plots of the angle-dependent polarized Raman peak intensities of A_g^2 mode as functions of sample

rotation angle, correspond to BP flakes in (a-c) under parallel polarization configurations, respectively.

References

[1] A. Brown,S. Rundqvist, *Acta Cryst.* **1965,** *19*, 684.

[2] J. Qiao,X. Kong,Z. X. Hu,F. Yang,W. Ji, *Nat. Commun.* **2014,** *5*, 4475.

[3] Z. X. Hu,X. Kong,J. Qiao,B. Normand,W. Ji, *Nanoscale* **2016,** *8*, 2740.

[4] S. Sugai,T. Ueda,K. Murase, *J. Phys. Soc. Jpn.* **1981,** *50*, 3356.

[5] S. Sugai,I. Shirotani, *Solid State Commun.* **1985,** *53*, 753.

[6] X. Ling,L. Liang,S. Huang,A. A. Puretzky,D. B. Geohegan,B. G. Sumpter,J. Kong,V. Meunier,M. S. Dresselhaus, *Nano Lett.* **2015,** *15*, 4080.

[7] C. Kaneta,H. Katayama-Yoshida,A. Morita, *J. Phys. Soc. Jpn.* **1986,** *55*, 1213.

[8] J. Ribeiro-Soares,R. M. Almeida,L. G. Can ̧cado,M. S. Dresselhaus,A. Jorio, *Phys. Rev. B* **2015,** *91*, 205421.

[9] J. W. Jiang,B. S. Wang,H. S. Park, *Journal of physics. Condensed matter : an Institute of Physics journal* **2016,** *28*, 165401.

[10] A. Castellanos-Gomez,L. Vicarelli,E. Prada,J. O. Island,K. L. Narasimha-Acharya,S. I. Blanter,D. J. Groenendijk,M. Buscema,G. A. Steele,J. V. Alvarez,H. W. Zandbergen,J. J. Palacios,H. S. J. van der Zant, *2D Materials* **2014,** *1*, 025001.

[11] H. B. Ribeiro,M. A. Pimenta,C. J. de Matos,R. L. Moreira,A. S. Rodin,J. D. Zapata,E. A. de Souza,A. H. Castro Neto, *ACS Nano* **2015,** *9*, 4270.

[12] X. Zhang,Q. H. Tan,J. B. Wu,W. Shi,P. H. Tan, *Nanoscale* **2016,** *8*, 6435.

[13] A. P. Scott,L. Radom, *The Journal of Physical Chemistry* **1996,** *100*, 16502.

[14] W. Lu,H. Nan,J. Hong,Y. Chen,C. Zhu,Z. Liang,X. Ma,Z. Ni,C. Jin,Z. Zhang, *Nano Research.* **2014,** *7*, 853.

[15] X. Ling,S. Huang,E. H. Hasdeo,L. Liang,W. M. Parkin,Y. Tatsumi,A. R. Nugraha,A. A. Puretzky,P. M. Das,B. G. Sumpter,D. B. Geohegan,J. Kong,R. Saito,M. Drndic,V. Meunier,M. S. Dresselhaus, *Nano Lett.* **2016,** *16*, 2260.

[16] Y. Cai,G. Zhang,Y. W. Zhang, *Sci. Rep.* **2014,** *4*, 6677.

[17] W. Setyawan,S. Curtarolo, *Comput. Mater. Sci.* **2010,** *49*, 299.

[18] J. Wu,N. Mao,L. Xie,H. Xu,J. Zhang, *Angew. Chem. Int. Ed.* **2015,** *54*, 2366.

[19] J. Kim,J. U. Lee,J. Lee,H. J. Park,Z. Lee,C. Lee,H. Cheong, *Nanoscale* **2015,** *7*, 18708.

[20] N. N. Mao,J. X. Wu,B. W. Han,J. J. Lin,L. M. Tong,J. Zhang, *Small* **2016,** *12*, 2627.